**Summary**

Extended common-image-point gathers can be constructed by wave-equation migration by preserving into the output image the non-zero lags of the cross-correlation between the source and receiver wavefields. Correct wavefield reconstruction leads to focused events in the extended CIPs, but incorrect reconstruction leads to defocused events that can be used for velocity model building. This approach limits the number of locations where the multi-lag cross-correlation needs to be computed, thus reducing the computational cost of this method while preserving its capacity to indicate velocity errors. The cheaper cost is particularly helpful when this method is used with wave-equation migration, especially with wide-azimuth data acquisition.

**Introduction**

Conventional seismic imaging methods share the fundamental assumption of single scattering at points of discontinuity in the subsurface. Under this assumption, waves used in imaging propagate from seismic sources, interact with discontinuities and return to the surface as reflected seismic waves. We commonly discuss about a "source" wavefield, originating at the seismic source and propagating in the medium prior to any interaction with discontinuities, and a "receiver" wavefield, originating at discontinuities and propagating in the medium to the receivers – the "WRW" model (Berkhout, 1982). The two wavefields are kinematically equivalent at discontinuities. Any mismatch between the wavefields indicates inaccurate wavefield reconstruction typically assumed to be due to inaccurate velocity. We do not need to make assumptions about up- or down-going propagation, since waves can move in any direction as long as they scatter only once; we do not need to make any assumption about how we reconstruct those two wavefields.

We can formulate imaging as a process involving two steps: the wavefield reconstruction and the imaging condition. The key elements in this imaging procedure are the source and receiver wavefields, $W_s$ and $W_r$. We can represent those wavefields as 4-dimensional objects, either in the time domain (for wavefield reconstruction using the two-way acoustic wave-equation) function of space $\mathbf{x} = \{x, y, z\}$ and time $t$, or in the frequency domain (for wavefield reconstruction using the one-way acoustic wave-equation) function of space and frequency $\omega$.

**Imaging conditions**

A conventional cross-correlation imaging condition (cIC) based on the reconstructed wavefields can be formulated in the time $t$ and frequency $\omega$ domains (Claerbout, 1985) as:

$$R(\mathbf{x}) = \sum_{shots} \sum_{t} W_s(\mathbf{x}, t)\, W_r(\mathbf{x}, t) \tag{1}$$

$$= \sum_{shots} \sum_{\omega} \overline{W_s(\mathbf{x}, \omega)} W_r(\mathbf{x}, \omega) \ , \tag{2}$$

where $R$ represents the migrated image. This operation defines the image as the zero lag (in space and time) of the cross-correlation between the two wavefields. This property holds under the assumption that the wavefields are kinematically equivalent at positions of discontinuity. An extended cross-correlation imaging condition (eIC) (Rickett and Sava, 2002; Sava and Fomel, 2006) defines the image as a function of space as well as the cross-correlation lags in space ($\boldsymbol{\lambda}$) and time ($\tau$). This imaging condition can also be formulated in the time and frequency domains:

$$R(\mathbf{x}, \boldsymbol{\lambda}, \tau) = \sum_{shots} \sum_{t} W_s(\mathbf{x} - \boldsymbol{\lambda}, t - \tau)\, W_r(\mathbf{x} + \boldsymbol{\lambda}, t + \tau) \tag{3}$$

$$= \sum_{shots} \sum_{\omega} \overline{W_s(\mathbf{x} - \boldsymbol{\lambda}, \omega)} W_r(\mathbf{x} + \boldsymbol{\lambda}, \omega)\, e^{2i\omega\tau} \ , \tag{4}$$

where the over-line represents complex conjugation. Equations 1-2 represents a special case of equations 3-4 for $\boldsymbol{\lambda} = 0$ and $\tau = 0$. The eICs defined by equations 3-4 can be used to analyze the accuracy

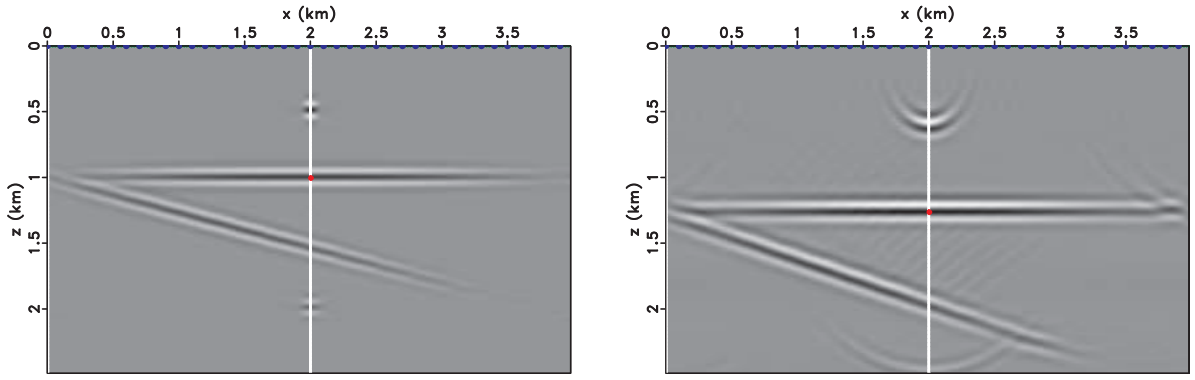


(a) (b)

Figure 1: Synthetic model with images constructed using (a) the correct velocity and (b) a velocity 20% faster throughout the model. The CIP cubes depicted in Figures 4(a)-4(c)-4(e) correspond to the diffractor and the horizontal and dipping reflectors at coordinates $z = \{0.50, 1.00, 1.50\}$ km when imaged with correct velocity, and at coordinates $z = \{0.75, 1.50, 2.00\}$ km when imaged with fast velocity.

of wavefield reconstruction. Assuming that all errors accumulated in the incorrectly-reconstructed wavefields are due to the velocity model, the extended images could be used for velocity model building using a tomographic approach.

The main problem with the eICs is that they require a large number of computations corresponding the the size of the image $\mathbf{x}$ and the number of space and time lags, $\boldsymbol{\lambda}$ and $\tau$. In practice, computing and saving the non-zero cross-correlation lags at all image coordinates is infeasible. Common approaches taken are to consider subsets of the extended images, for example horizontal space-lag images $R(\mathbf{x}, \lambda_x, \lambda_y)$, vertical space-lag images $R(\mathbf{x}, \lambda_z)$, time-lag images $R(\mathbf{x}, \tau)$, etc. In all cases, the cross-correlation lags, sometimes referred-to as subsurface offsets, are computed at discrete locations in the image and then analyzed in common-image-gathers, for example $R(z, \lambda_x, \lambda_y)$, $R(x, y, \lambda_z)$, or $R(z, \tau)$, etc. Sometimes, this analysis is performed in the angle domain constructed, for example, by the method of Sava and Fomel (2003).

**Extended common-image-point gathers**

In this paper, we consider the case of extended images extracted at locations in the image volume where a reflector or diffractor are present, i.e. consider a fixed coordinate $\mathbf{x}$. The question is whether the information provided by the eICs at a single point characterizes the accuracy of wavefield reconstruction and is usable for velocity updates. The events depicted in extended CIPs at a given position correspond to wavefields originating at that point and propagating in the vicinity of this point using the local medium parameters (Vasconcelos et al., 2009).

Consider the images depicted in Figures 1(a)-1(b) created from the same synthetic dataset using correct and fast velocities. Figures 3(a)-3(c)-3(e) depict the extended CIPs for 3 shots located on the surface and imaged with the correct velocity. The CIPs depict planar events which include the zero-lag point. The superposition of CIPs similar to the ones shown here for all shots on the surface generates the CIP shown in Figure 4(c). We observe a focused event in the $\lambda_x - \tau$ panel indicating correct imaging. In contrast, Figures 3(b)-3(d)-3(f) depict the extended CIPs for the same 3 shots, but imaged using the fast velocity. The CIPs depict non-planar which do not pass through the zero-lag point. The superposition of CIPs similar to the ones shown here for all shots on the surface generates the CIP shown in Figure 4(d). We observe an event with moveout in the $\lambda_x - \tau$ panel indicating incorrect imaging.

A similar analysis is possible for other events in the image, as shown in Figures 4(a)-4(b) for the diffractor and in Figures 4(e)-4(f) for the dipping reflector. In all cases, an essential component of the CIPs is the time-lag axis which allows the analysis of focusing and defocusing indicating the accuracy of wavefield reconstruction. Furthermore, the vertical lag axis $\lambda_z$ does not carry much information for horizontal reflectors, but can potentially be used to evaluate structural dip, as can be seen by comparing

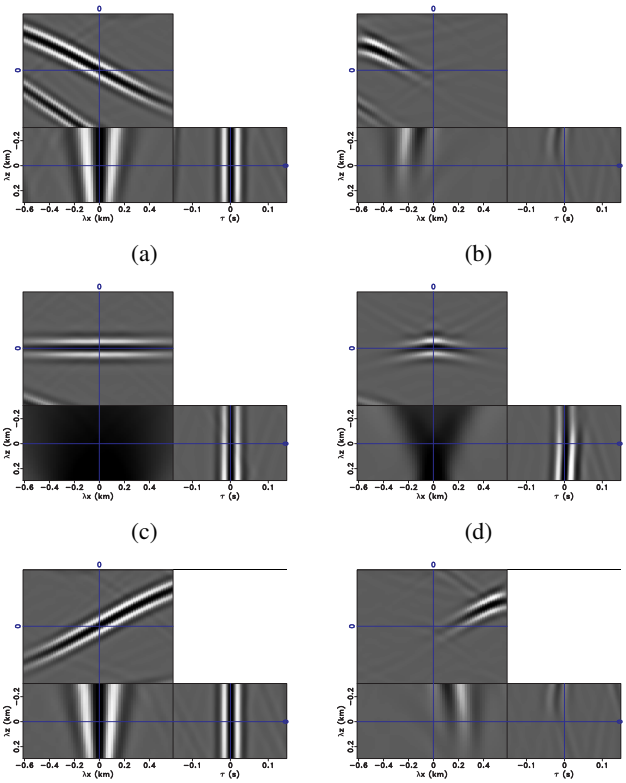


Figure 2: Extended common-image-point gathers corresponding to migration with correct velocity (panels a,c,e) and fast velocity (panels b,d,f). All panels correspond to the horizontal reflector. Panels (a,b) correspond a shot at $x = 1.5$ km, (c,d) to a shot at $x = 2.0$ km and (e,f) to a shot at $x = 2.5$ km. The cubes depict CIPs function of space-lags $\lambda_z, \lambda_x$ and time-lag $\tau$. The slices shown intersect in the middle of the cubes, i.e. at zero cross-correlation lags.

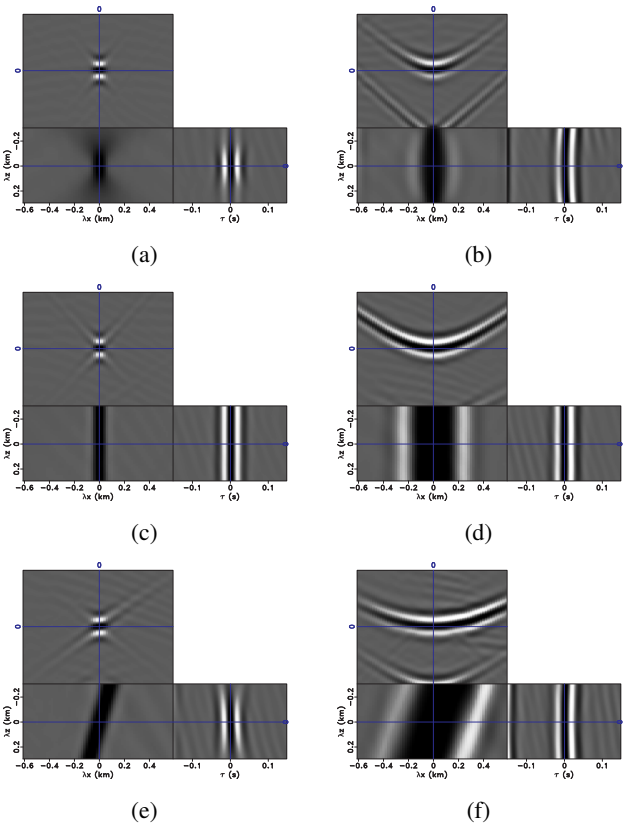


Figure 3: Extended common-image-point gathers corresponding to migration with correct velocity (panels a,c,e) and fast velocity (panels b,d,f). Panels (a,b) correspond to the diffractor, (c,d) to horizontal reflector and (e,f) to the dipping reflector. The eICs correspond to all the shots located on the surface. The cubes depict CIPs function of space-lags $\lambda_z, \lambda_x$ and time-lag $\tau$. The slices shown intersect in the middle of the cubes, i.e. at zero cross-correlation lags. The value at zero lags represents the conventional image shown in Figures 1(a)-1(b).

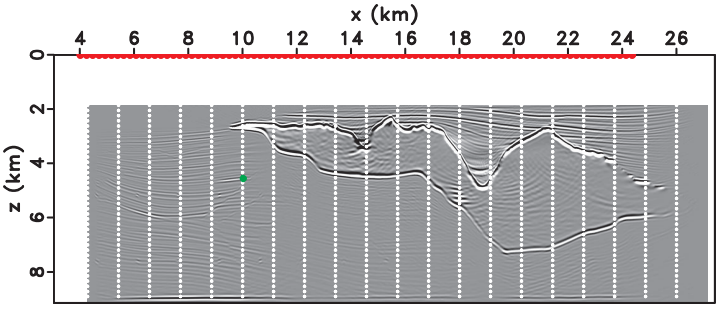


Figure 4: Sigsbee 2A migrated image using correct velocity. The dots overlain on the image indicate the locations of extended CIPs. The dots on the surface indicate the locations of the shots used for imaging.

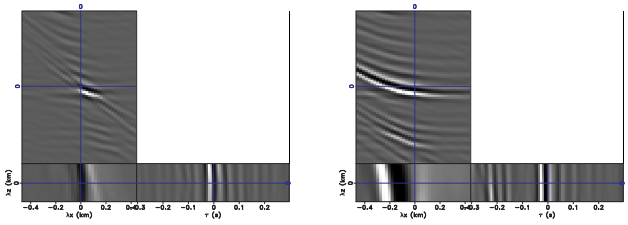

(a) (b)

Figure 5: Extended CIPs corresponding to (a) correct and (b) fast velocities. The events are truncated due to the off-end acquisition of surface data.

Figures 4(c) and 4(e). Focusing in the lag domain allows for separation reflectors and diffractors, as can be seen by comparing Figures 4(e) and 4(a). In all cases, the comparison assumes that imaging is done with correct velocity.

This analysis is applicable to more complex models, e.g. Sigsbee 2A (Paffenholz et al., 2002). Figure 4 shows the migrated image using the conventional IC. The dots overlain on the image indicate the locations where extended CIPs are computed. Figures 6(a)-6(b) depict the extended CIPs for a reflector which is in the image constructed with correct velocity is located at coordinates $\{x, z\} = \{10.0, 4.5\}$ km. The two CIPs correspond to imaging with correct (6(a)) and incorrect velocities (6(b)). As in the preceding example, the events are focused in the $\lambda_x - \tau$ panels when imaged with correct velocity, but defocus when imaged with incorrect velocity. The events are partially truncated because the off-end acquisition of the data on the surface.

## Conclusions

Extended common-image-point gathers are effective tools for analyzing velocity accuracy for wave-equation imaging. The extended CIPs can be computed and analyzed at sparse locations in the image volume, thus drastically reducing the computational cost of this method.

## Acknowledgments

Paul Sava acknowledges the support of the sponsors of the Center for Wave Phenomena at Colorado School of Mines. Ivan Vasconcelos acknowledges ION Geophysical for support of this research.

## REFERENCES

Berkhout, A. J., 1982, Imaging of acoustic energy by wave field extrapolation: Elsevier.

Claerbout, J. F., 1985, Imaging the Earth's interior: Blackwell Scientific Publications.

Paffenholz, J., B. McLain, J. Zaske, and P. Keliher, 2002, Subsalt multiple attenuation and imaging: Observations from the Sigsbee2B synthetic dataset: 72nd Annual International Meeting, SEG, Soc. of Expl. Geophys., 2122–2125.

Rickett, J., and P. Sava, 2002, Offset and angle-domain common image-point gathers for shot-profile migration: Geophysics, **67**, 883–889.

Sava, P., and S. Fomel, 2003, Angle-domain common image gathers by wavefield continuation methods: Geophysics, **68**, 1065–1074.

———, 2006, Time-shift imaging condition in seismic migration: Geophysics, **71**, S209–S217.

Vasconcelos, I., P. Sava, and H. Douma, 2009, Image-domain interferometry and extended images: Presented at the 71st Mtg., Abstracts, Eur. Assoc. Expl. Geophys.